# Fluid-like Surface Layer and Its Flow Characteristics in Glassy Nanotubes

Matthew C. Wingert,[†] Soonshin Kwon,[†] Shengqiang Cai,*,[†] and Renkun Chen*,[†]

[†]Department of Mechanical and Aerospace Engineering, University of California, San Diego, La Jolla, California 92093, United States

Ⓢ Supporting Information

ABSTRACT: We show that amorphous silica and Si nanotubes can flow at room temperature under Giga-Pascal order stress when going to the nanometer scale. This creep behavior is unique for the amorphous nanotubes and is absent in crystalline Si nanotubes of similar dimensions. A core−shell model shows that there exists an approximately 1 nm thick viscoelastic "fluid-like" surface layer, which exhibits a room temperature viscosity equivalent to that of bulk glass above 1000 °C.
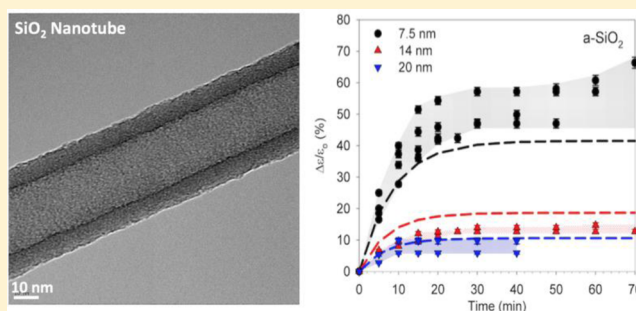
KEYWORDS: Glass transition, silica nanotube, silicon nanotube, viscoelasticity, creep strain, core-shell model

Nanoscale glassy films are ubiquitous and critical components for a variety of electronic and energy devices such as optical coatings,[1−3] amorphous oxide transistors[4,5] and gate dielectrics,[6−8] nonvolatile solid state memory,[9,10] memristors,[11−13] solid-electrolyte interphase layers[14] and anodes[15,16] in batteries, and amorphous Si solar cells.[17,18] The mechanical properties of such amorphous materials are practically important in system design and issues can arise when shrinking them down to nanoscale dimensions. For instance, in glassy polymers, extensive studies have shown the presence of a highly mobile surface layer on the order of tens of nanometers thick.[19−26] In the case of glassy (or amorphous) inorganic materials, whether or not a similar surface layer exists, however, is largely unexplored. A prior study has indicated such a possibility through imaging the motion of surface atoms in ultrathin SiO_2 films,[27,28] but its effect on the dynamic mechanical properties is not known. On the other hand, it is well-known that inorganic nanostructures in both amorphous and crystalline forms can exhibit unusual mechanical phenomena, such as electron beam-induced deformation,[29−31] brittle-plastic transition,[32−34] and strong anelasticity (atomic diffusion).[35] It is, therefore, expected that if a mobile surface layer does exist, the mechanical behavior of nanostructured glass could be different from that of its bulk form. One of the challenges of directly probing the dynamic mechanical response of this surface layer lies in creating and measuring ultrathin samples, as the mobile surface layer, if it exists, would be on the scale of several nanometers, much smaller than that in polymers.

Herein, we systematically studied the dynamic mechanical behavior of novel amorphous SiO_2 (a-SiO_2) and Si (a-Si) nanotube (NT) structures with exceedingly thin shells down to 7 nm (Figure 1), unambiguously showing the presence of
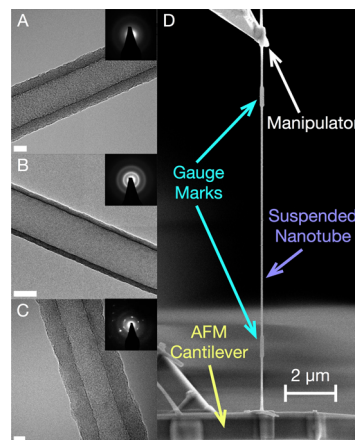

Figure 1. TEM images of individual ultrathin (a) amorphous SiO_2, (b) amorphous Si, and (c) crystalline Si nanotube (NT) samples, and (d) SEM of tensile creep experimental setup. Scale bars are (a) 10, (b) 50, and (c) 5 nm.

highly mobile surface layers in inorganic glasses. The thin shells and high aspect-ratio of the tubular structure, having increased surface atom fraction, allow us to apply large stresses (10^9 Pa) and examine the mechanical behavior. Exponentially increasing creep deformation at room temperature is observed as the NT shell thickness is reduced, with strain increases up to 60% greater than the initial strain (<5.5%) for the thinnest tubes. We also observed that creep deformation occurs only in the amorphous samples we studied (a-SiO_2 and a-Si NTs) and not
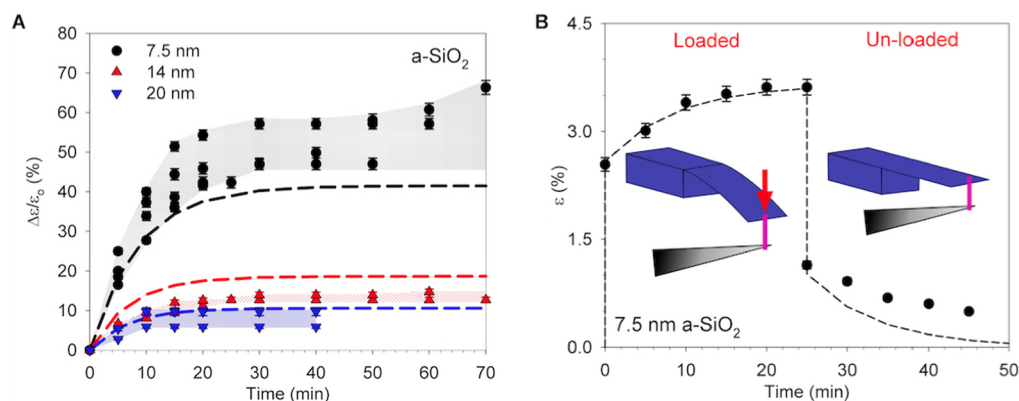
Figure 2. Creep behavior of a-SiO$_2$ nanotube (NTs). (a) Creep strain measured for a-SiO$_2$ NTs. Colored bands represent the range of the experimental data for similar shell thickness NTs. (b) Viscoelastic behavior of a 7.5 nm shell a-SiO$_2$ NT. The insets show schematics of the loading and unloading of the NT with the AFM cantilever. The dashed lines in (a) and (b) represent fittings based on eq 5. Initial applied stress is ~1 GPa (see Supporting Information Figure S5).
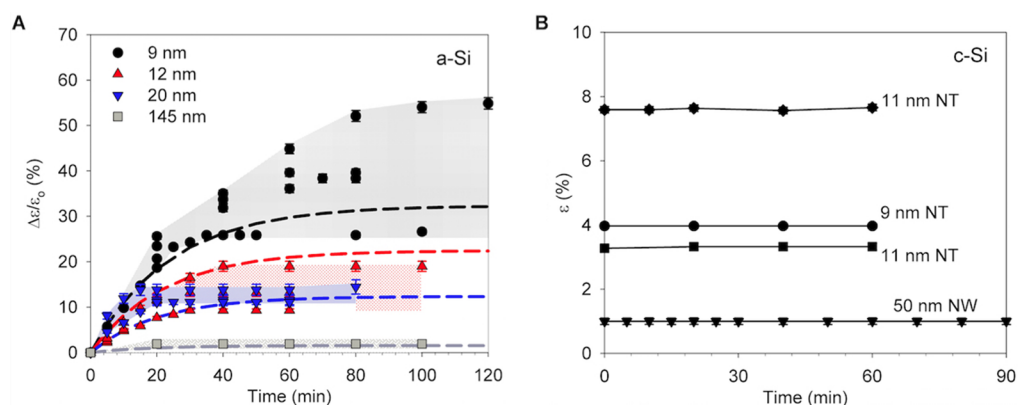
Figure 3. (a) Creep strain measured for a-Si NTs. The dashed lines represent fittings based on eq 5. (b) No creep was observed for crystalline Si (c-Si) NTs or nanowires (NWs). Initial applied initial stresses range from 1 to 5 GPa for a-Si NTs and 1.4 to 2.4 GPa for c-Si NTs and NWs (see Supporting Information Figure S5).

in crystalline Si (c-Si) NTs of similar geometry. Furthermore, we performed temperature dependent creep tests and found a low diffusion-like activation energy associated with the creep.

The ultrathin NTs in this study were fabricated by etching the Ge cores in Ge–Si core–shell nanowires (NWs)[36] as we previously reported, where crystalline and amorphous NTs were fabricated by controlling the temperature during epitaxial deposition of the Si shells on the Ge cores.[37] Amorphous SiO$_2$ NTs were synthesized by oxidizing c-Si NTs in air at 950 °C for 3 h and are completely oxidized with no internal interfaces while the a-Si and c-Si NTs have 1–2 nm thick inner and outer native oxide coatings encompassing the Si shells. NT shell thicknesses ranged from ~7.5, 12, and 20 nm for a-SiO$_2$, ~9, 12, 20, and 150 nm for a-Si, and ~10 nm for c-Si, ±2 nm each, with deviations of <1 nm along the NT length. The outer diameters (ODs) of the NTs range from ~70–150 nm. Each NT was characterized by high-resolution transmission electron microscopy (HRTEM) (representative images in Figure 1a–c with larger NTs shown in Supporting Information[38]) prior to tensile testing in order to confirm the crystallinity of the sample and to precisely measure its dimensions (OD, shell thickness, and native oxide thickness for the a-Si and c-Si NTs).

After TEM characterization, the same exact NTs were then transferred to a dual (electron and ion) beam chamber where a micromanipulator probe was used to pick up and attach each NT to the free end of an AFM cantilever. Tensile measure-

ments were then performed according to an established procedure[37,39] using the setup shown in Figure 1d. During the initial loading, stress–strain measurements were performed to calculate instantaneous tensile moduli,[38] which were consistent with those of SiO$_2$,[40−42] a-Si,[43] and c-Si nanostructures,[44] including our previously measured NTs.[37] Each of these initial measurements only took 2–3 min and was performed in the linear-elastic regime with strains and stresses up to 1.5–5.5% and 0.8–5 GPa, respectively.[38] Such large stresses can only be sustained when the nanostructure has a low volumetric concentration of defects to avoid fracturing, as shown by the high fracture strength of our NTs.[38] Transient creep was then monitored with the NT at the maximum loaded stress by measuring changes in length every 5 to 10 min over a period of up to 2 h, blanking the electron beam between measurements.

Some of the samples had gauge marks deposited via e-beam induced Pt (seen in Figure 1d) and strain was measured using both the gauge marks and the entire NT length to ensure no slippage occurred. There was no observable difference in the strain–stress and creep measurement results between the samples with and without the gauge marks. Additionally, we did not observe any localized deformation in the NTs near gauge marks. These experiments indicate that the deposition of the gauge mark did not influence the measurements. Temperature-dependent creep tests were also performed in situ in the same
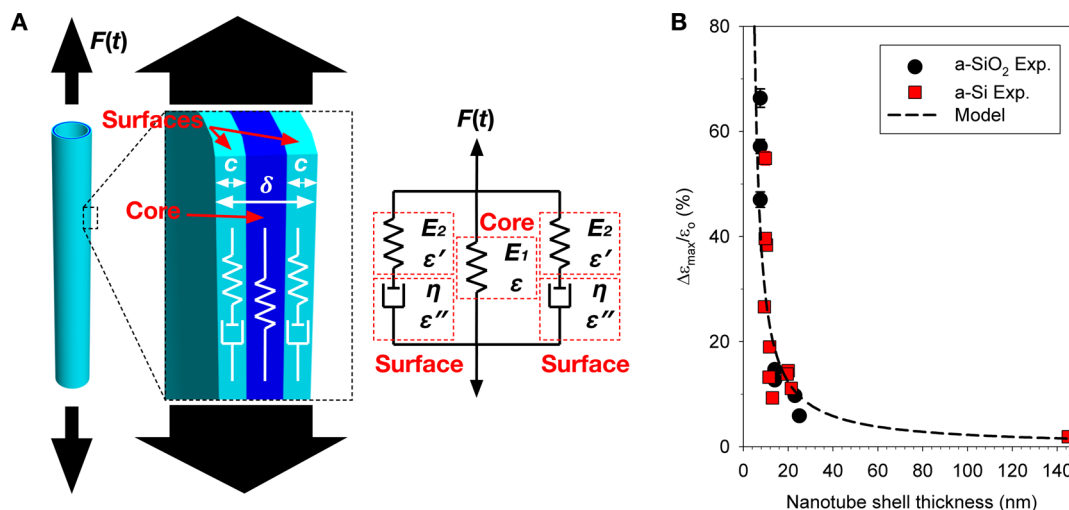
Figure 4. (a) Core−shell model describing the dynamic and size-dependent behavior of the amorphous nanotubes and (b) the experimental (circles and squares) and modeled (dashed line) size-dependent normalized saturated creep.

chamber, where a heater implanted in the sample stage was used to control the temperature above 300 K and the sample temperature was measured with a thermometer.

The creep strain measured in the a-SiO$_2$ NTs is shown in Figure 2a, where the strain increase due to creep, $\Delta\varepsilon$, is normalized by the initial strain, ε_o. The majority of the creep occurred within the first 20−30 min and saturated thereafter. The creep is clearly related to the a-SiO$_2$ NT shell thickness (δ), where $\Delta\varepsilon/\varepsilon_o$ only reaches 10% for NTs with $\delta > 10$ nm but is as high as 60% when $\delta < 10$ nm. The viscoelastic response of the 7.5 nm a-SiO$_2$ NTs was studied by continuously measuring the strain after the applied stress was unloaded following creep saturation with a representative measurement shown in Figure 2b. Most of the creep strain was recovered over the next 30 min, indicating that the creep deformation in this study is viscoelastic, as opposed to previously observed[34] enhanced plastic deformation that occurred above a threshold yield-stress and with larger strain (typically ∼10%).

To examine if the observed creep behavior was unique in a-SiO$_2$, we also performed similar tests on amorphous and crystalline Si NTs. The a-Si NTs exhibit a similar amount of creep in terms of overall strain increase and size-dependence, shown in Figure 3a. This similarity between the ultrathin a-SiO$_2$ and a-Si NTs indicates that a-Si indeed exhibits glass-like behavior, as has been previously suggested.[45,46] The creep saturation in the a-Si NTs, however, took longer than in the a-SiO$_2$ NTs. Negligible creep was observed in a 145 nm thick a-Si NT, as expected for bulk-like behavior. Interestingly, no creep was observed in ∼10 nm thick crystalline Si NTs (Figure 3b), which have the same native oxide surface layers as the a-Si NTs (see Supporting Information Table S1), just like in our control experiment on a 50 nm diameter c-Si NW.

The size-dependent creep observed in Figures 2a and 3a is presumably due to the growing influence of a fluid-like surface layer on the amorphous nanostructures, similar to that of the thin mobile surface layers in amorphous polymer films. As such, we used a core−shell model, similar to a Maxwell-solid spring-dashpot system (Figure 4a), to understand the observed behavior, where the NT shell is comprised of mobile surfaces surrounding a stiff center layer. The model neglects some characteristics of complex fluid such as threshold stress of flow,

however, we adopted the spring dashpot model because it is probably the simplest model with the minimum number of fitting parameters.

Here, the time dependent mechanical response of the NT under the influence of a tensile force, $F(t)$, is

$$F(t) = E_1\varepsilon(t)A_{core} + E_2\varepsilon'(t)A_{surf} \tag{1}$$

where the stiff middle layer has a modulus, E_1, cross-sectional area, A_{core}, and experiences a strain, $\varepsilon(t)$, while the fluid-like surface layers have elastic moduli, E_2, of the Maxwell model, total cross-sectional area, A_{surf}, and experience a strain, $\varepsilon'(t)$. The average stress over the entire cross-section of the NT with a total shell thickness of δ and inner/outer surface layers, each of thickness c, is

$$\bar{\sigma}(t) = E_1\varepsilon(t)\left(1 - \frac{2c}{\delta}\right) + E_2\varepsilon'(t)\left(\frac{2c}{\delta}\right) \tag{2}$$

and the elastic and viscous contributions in the inner/outer surface layers are related by

$$E_2\varepsilon'(t) = \eta\dot{\varepsilon}''(t) \tag{3}$$

where η is the viscosity of the surface layer and $\varepsilon''(t)$ is the viscous strain. By combining eqs 2 and 3 and the fact that the average stress is kept constant during the creep test, we obtain

$$\ddot{\varepsilon}(t) + \frac{E_1\left(1 - \frac{2c}{\delta}\right)}{E_1\left(1 - \frac{2c}{\delta}\right) + E_2\left(\frac{2c}{\delta}\right)}\frac{1}{\tau}\dot{\varepsilon}(t) = 0 \tag{4}$$

The solution of the above equation is

$$\frac{\varepsilon(t)}{\varepsilon_o} = 1 + \frac{E_2\left(\frac{2c}{\delta}\right)}{E_1\left(1 - \frac{2c}{\delta}\right)} - \left[\frac{E_2\left(\frac{2c}{\delta}\right)}{E_1\left(1 - \frac{2c}{\delta}\right)}\right]$$

$$\exp\left[-\frac{E_1\left(1 - \frac{2c}{\delta}\right)}{E_1\left(1 - \frac{2c}{\delta}\right) + E_2\left(\frac{2c}{\delta}\right)}\left(\frac{t}{\tau}\right)\right] \tag{5}$$

where the time constant is defined as $\tau = \eta/E_2$ and the normalized maximum creep strain is
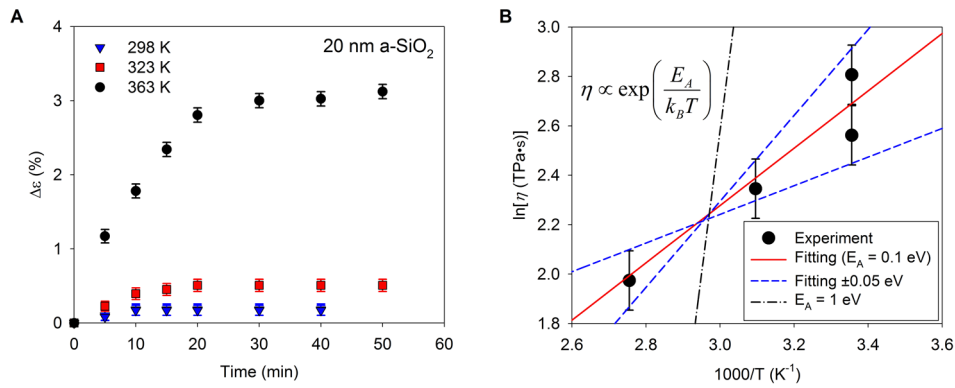
Figure 5. (a) Creep strain observed for 20 nm shell amorphous SiO_2 nanotubes at various temperatures. (b) Creep viscosity versus temperature, fitted to an Arrhenius temperature dependence with an activation energy of $E_A = 0.1 \pm 0.05$ eV, consistent with bond motion/rearrangement. For comparison, temperature-dependent viscosity requiring an activation energy of 1 eV, signifying a bond breaking mechanism, is shown.

$$\frac{\Delta\varepsilon_{max}}{\varepsilon_o} = \frac{E_2}{E_1}\left(\frac{2c}{\delta - 2c}\right) \tag{6}$$

We assumed that $E_1 \approx E_2$, based on the size-independent instantaneous modulus[38] (Figure S4A) measured for the amorphous NTs, and eq 2 at $t = 0$ ($\varepsilon = \varepsilon'$) and found that a surface layer thickness (c) of 1.1 nm best fits the experimental data for both amorphous NT materials, which is reasonable considering that the mobile surface layers should be on the order of nanometers. The creep calculated from eq 5 and represented by the dashed lines in Figures 2a and 3a, matches the measured time-dependence trends of the creep fairly well. The initial creep shown in Figure 2b also fits well to eq 5, where the initial starting strain was calculated as the ratio of the initial stress and elastic modulus, $\varepsilon_o = \sigma_o/E_1$. The creep recovery after stress removal is simply

$$\varepsilon_{recovery}(t) = \Delta\varepsilon_{max} \exp\left[-\frac{E_1\left(1-\frac{2c}{\delta}\right)}{E_1\left(1-\frac{2c}{\delta}\right) + E_2\left(\frac{2c}{\delta}\right)}\left(\frac{t - t_c}{\tau}\right)\right] \tag{7}$$

where $\Delta\varepsilon_{max}$ is defined from eq 6 and t_c is the time at which the stress was removed. Here, the time constant that best fit the a-SiO_2 and a-Si NTs was 6 and 18 min, respectively. The corresponding viscosity of the soft outer/inner layers can be estimated from $\eta = \tau E_2$ and was ∼10−20 TPa·s for the a-SiO_2 NTs at room temperature, equivalent to the viscosity of glass measured[47,48] between 1250 and 1500 K, and ∼60−90 TPa·s for the a-Si NTs. This is an astonishingly low viscosity at room temperature for inorganic glass, given the exponential dependence of viscosity on temperature. One would not have predicted a priori the order of magnitude of room-temperature viscosity of these surface layers in a-SiO_2 and a-Si, given the fact that the highly mobile layer in glassy polymers occurred at a temperature (room temperature) only a few tens of degree Kelvin below their glass transition temperature.

The size-dependence of the creep deformation is more clearly evident in Figure 4b, where $\Delta\varepsilon_{max}/\varepsilon_o$ is plotted against NT shell thickness. The a-SiO_2 and a-Si NTs follow strikingly similar size-dependent trajectories with the maximum creep largely increasing as the NT shell thickness decreases. The observed creep trends only with the NT thickness and is independent of testing parameters such as the initial strain and stress.[38] The dashed lines represent the modeled saturation creep strain based on eq 6 using the same constants previously

mentioned and shows good agreement with the experimental data. Interestingly, if we calculate the relaxed tensile modulus using the saturated total strain,[38] we find that it decreases as δ falls below 30 nm for a-Si, similar to the size-dependent moduli of c-Si NTs[37] and NWs.[39]

Differences in the saturation time between the a-SiO_2 and a-Si NTs, however, may stem from a difference in atomic species mobility in either material. It is also possible that the a-SiO_2/a-Si interface, present in the a-Si NTs and a source of atomic defects and roughness,[37] may reduce the overall atomic mobility and increase the time required for the atoms to reorganize. Furthermore, the lack of any creep in the c-Si NTs, even with similar geometry as the a-Si NTs and with native surface oxides, also highlights the importance of the exact nature of this interface. This could be caused by the presence of a higher density layer at the c-Si/SiO_2 interface (∼1 nm thick),[49] or atoms in the native surface oxide, near to the interface with the ordered crystalline surface, could be more ordered, confining and inhibiting their movement.[50] However, understanding the exact role of the interfaces among the a-SiO_2, a-Si, and c-Si NTs warrants further investigation.

It is also worth noting that we did not notice any surface roughening phenomena during our experiments. We think it is probably because our observation time is relatively short. For the fluid-like surface layer, only local rearrangement of atoms is required to relax the stress, which takes relatively short time. To develop visible instability patterns such as Rayleigh−Plateau instability or Asaro−Tiller−Grinfeld instability on the NT surface, global transportation of atoms are necessary, which should take much longer time. Examining possible surface instability patterns in a-Si and a-SiO2 NTs subjected to external stress in much longer time scale will be an interesting future direction of our studies.

To understand the mechanism behind the surface-based creep, we performed temperature-dependent creep tests on 20 nm thick SiO_2 NTs (Figure 5a) and found that the amount of creep significantly increased with temperature; however, τ remained constant. The resulting creep viscosity was found to fit well to an Arrhenius temperature dependence[51] (Figure 5b)

$$\eta = E_2\tau \propto \exp\left(\frac{E_A}{k_B T}\right) \tag{8}$$

where k_B is the Boltzmann constant and T is absolute temperature. The activation energy of the deformation processes, E_A, was found to be 0.1 ± 0.05 eV, of similar

order as low values for diffusion and defect relaxation (~0.2 eV) in a-Si[52−54] and a-SiO₂.[55] Furthermore, activation energies could be lower for the fluid-like surface, similar to values simulated for SiO₂ surfaces.[56,57] These energies are consistent with analysis[58] showing deformation at room temperature requires activation energies less than 0.3 eV and indicate that bond motion, not bond breaking,[59] is the source of the measured creep.

On the basis of our low observed activation energy, the creep deformation in the amorphous NTs is most likely due to multiple defected bond relaxation events that result in the migration of atomic clusters.[60,61] Such reorganizations will alter coordinated bonding groups, rings of Si−O molecules in a-SiO₂ or Si−Si in a-Si, such as transforming five- and six-fold coordinated group rings into three-, four-, and eight-member coordinated groups[62] and migration of nonbridging atoms leading changes in bond angles.[60] This atomic reordering is particularly concentrated at surfaces, where natural defects such as dangling bonds allow atomic processes to circumvent the higher energy barriers present among the bulk atoms, leading to the high mobility of the surface layers. Because our NTs are made up of a significant fraction of surface atoms, they will increasingly govern the mechanical response of the entire nanostructure, as observed in in our experiments.

Deformation in prior studies on SiO₂ and Si nanostructures was investigated using constant strain rates[33,34] or high energy electron beams[29−31] which break atomic bonds and dislocate atoms. One such recent study[34] found that sub-20 nm diameter a-SiO₂ nanofibers show ductile behavior and enhanced plastic elongation above a threshold yield-stress. Our results, however, were performed in the elastic range,[38] and while we show similar strong size-dependent deformation, it occurs significantly below the yield-stress and is viscoelastic, recovering the majority of the creep upon removal of the tensile load. Also in this study, the 5 kV electron beam will only transfer <0.4−0.7 eV to atoms in our nanostructures,[63] which is much lower than the energy required to break Si−O or Si−Si bonds (~2−5 eV)[64] but could have some influence on our measurement due to our measured E_A = 0.1 ± 0.05 eV. TEM irradiation in previous studies is much stronger, 100−300 kV beams can transfer ~9−33 eV,[63] strong enough to continuously create defects. We took further precaution by blanking the beam between measurements. Heating of the nanostructure should be negligible under a periodically scanning 5 kV beam. Stresses on the order of 10⁹ Pa, as applied in our experiments,[38] are also large enough to initiate defect bond rearrangements, providing >0.4 eV compared to our 0.1 ± 0.05 eV.

We observed strongly size-dependent creep deformation in ultrathin amorphous nanostructures, which was viscoelastic and not solely plastic in nature, nor limited by a threshold yield-stress. This same time- and size- dependent behavior did not occur in crystalline structures with similar geometry and native surface oxide. Furthermore, a core−shell model shows that an ~1 nm thick fluid-like surface layer has a significant effect on mechanical behavior and matches well with our experimental results. Additionally, a low activation energy extracted from temperature-dependent creep measurements indicates that the deformation is due to bond motionand not bond breaking. These findings show that the mobility of surfaces must be accounted for in nanoscale amorphous systems. Such behavior could have major implications for the design and functionalities of future electronic and energy devices.

■ ASSOCIATED CONTENT

Ⓢ Supporting Information

The Supporting Information is available free of charge on the ACS Publications website at DOI: 10.1021/acs.nano-lett.6b03377.

Geometric information on all the nanotube samples, TEM images of the nanotubes, representative stress−strain curve, instantaneous and relaxed moduli of the nanotubes, dependence of maximum creep strain increase on initial applied stress and strain, measured fracture strength of a-Si NTs, temperature dependent viscosity, and effect of electron beam exposure (PDF)

■ AUTHOR INFORMATION

Corresponding Authors
*E-mail: shqcai@ucsd.edu.
*E-mail: rkchen@ucsd.edu.

Author Contributions
M.C.W and S. K contributed equally to this work.

Notes
The authors declare no competing financial interest.

■ ACKNOWLEDGMENTS

■ REFERENCES

(1) Du, Y.; Luna, L. E.; Tan, W. S.; Rubner, M. F.; Cohen, R. E. *ACS Nano* **2010**, *4* (7), 4308−4316.

(2) Kats, M. A.; Blanchard, R.; Genevet, P.; Capasso, F. *Nat. Mater.* **2012**, *12* (1), 20−24.

(3) Klein, L. C. *Sol-gel optics: processing and applications*; Springer Science & Business Media: New York, 2013; Vol. 259.

(4) Nomura, K.; Ohta, H.; Takagi, A.; Kamiya, T.; Hirano, M.; Hosono, H. *Nature* **2004**, *432* (7016), 488−492.

(5) Kamiya, T.; Nomura, K.; Hosono, H. *Sci. Technol. Adv. Mater.* **2010**, *11* (4), 044305.

(6) Pal, B. N.; Dhar, B. M.; See, K. C.; Katz, H. E. *Nat. Mater.* **2009**, *8* (11), 898−903.

(7) Liu, J.; Buchholz, D. B.; Hennek, J. W.; Chang, R. P. H.; Facchetti, A.; Marks, T. J. *J. Am. Chem. Soc.* **2010**, *132* (34), 11934−11942.

(8) Wong, H.; Iwai, H. *Microelectron. Eng.* **2006**, *83* (10), 1867−1904.

(9) Raoux, S.; Xiong, F.; Wuttig, M.; Pop, E. *MRS Bull.* **2014**, *39* (08), 703−710.

(10) Fujisaki, Y. *Jpn. J. Appl. Phys.* **2013**, *52* (4R), 040001.

(11) Miao, F.; Strachan, J. P.; Yang, J. J.; Zhang, M.-X.; Goldfarb, I.; Torrezan, A. C.; Eschbach, P.; Kelley, R. D.; Medeiros-Ribeiro, G.; Williams, R. S. *Adv. Mater.* **2011**, *23* (47), 5633−5640.

(12) Liu, D.; Cheng, H.; Zhu, X.; Wang, G.; Wang, N. *ACS Appl. Mater. Interfaces* **2013**, *5* (21), 11258−11264.

(13) Wang, Z. Q.; Xu, H. Y.; Li, X. H.; Yu, H.; Liu, Y. C.; Zhu, X. J. *Adv. Funct. Mater.* **2012**, *22* (13), 2759−2765.

(14) Zhou, D.; Liu, R.; He, Y.-B.; Li, F.; Liu, M.; Li, B.; Yang, Q.-H.; Cai, Q.; Kang, F. *Advanced Energy Materials* **2016**, *6*, 1502214.

(15) Wu, H.; Chan, G.; Choi, J. W.; Ryu, I.; Yao, Y.; McDowell, M. T.; Lee, S. W.; Jackson, A.; Yang, Y.; Hu, L.; Cui, Y. *Nat. Nanotechnol.* **2012**, *7* (5), 310−315.

(16) Yao, Y.; McDowell, M. T.; Ryu, I.; Wu, H.; Liu, N.; Hu, L.; Nix, W. D.; Cui, Y. *Nano Lett.* **2011**, *11* (7), 2949−2954.

(17) Kondo, M.; Matsui, T.; Nasuno, Y.; Sonobe, H.; Shimizu, S. *Thin Solid Films* **2006**, *501* (1−2), 243−246.

(18) Shah, A.; Torres, P.; Tscharner, R.; Wyrsch, N.; Keppner, H. *Science* **1999**, *285* (5428), 692−698.

(19) Fakhraai, Z.; Forrest, J. A. *Science* **2008**, *319* (5863), 600−604.

(20) Chai, Y.; Salez, T.; McGraw, J. D.; Benzaquen, M.; Dalnoki-Veress, K.; Raphaël, E.; Forrest, J. A. *Science* **2014**, *343* (6174), 994−999.

(21) Yang, Z.; Fujii, Y.; Lee, F. K.; Lam, C.-H.; Tsui, O. K. C. *Science* **2010**, *328* (5986), 1676−1679.

(22) Yin, H.; Madkour, S.; Schönhals, A. *Macromolecules* **2015**, *48* (14), 4936−4941.

(23) Ellison, C. J.; Torkelson, J. M. *Nat. Mater.* **2003**, *2* (10), 695−700.

(24) Zhu, L.; Brian, C. W.; Swallen, S. F.; Straus, P. T.; Ediger, M. D.; Yu, L. *Phys. Rev. Lett.* **2011**, *106* (25), 256103.

(25) Brian, C. W.; Yu, L. *J. Phys. Chem. A* **2013**, *117* (50), 13303−13309.

(26) Forrest, J. A.; Dalnoki-Veress, K. *ACS Macro Lett.* **2014**, *3* (4), 310−314.

(27) Huang, P. Y.; Kurasch, S.; Alden, J. S.; Shekhawat, A.; Alemi, A. A.; McEuen, P. L.; Sethna, J. P.; Kaiser, U.; Muller, D. A. *Science* **2013**, *342* (6155), 224−227.

(28) Heyde, M. *Science* **2013**, *342* (6155), 201−202.

(29) Zheng, K.; Wang, C.; Cheng, Y.-Q.; Yue, Y.; Han, X.; Zhang, Z.; Shan, Z.; Mao, S. X.; Ye, M.; Yin, Y.; Ma, E. *Nat. Commun.* **2010**, *1*, 1.

(30) Zhu, X.; Su, J.; Wu, Y.; Wang, L.; Wang, Z. *Nanoscale* **2014**, *6* (3), 1499−1507.

(31) Dai, S.; Zhao, J.; Xie, L.; Cai, Y.; Wang, N.; Zhu, J. *Nano Lett.* **2012**, *12* (5), 2379−2385.

(32) Kim, Y.-J.; Lee, W. W.; Choi, I.-C.; Yoo, B.-G.; Han, S. M.; Park, H.-G.; Park, W. I.; Jang, J.-i. *Acta Mater.* **2013**, *61* (19), 7180−7188.

(33) Yue, Y.; Zheng, K. *Appl. Phys. Lett.* **2014**, *104* (23), 231906.

(34) Luo, J.; Wang, J.; Bitzek, E.; Huang, J. Y.; Zheng, H.; Tong, L.; Yang, Q.; Li, J.; Mao, S. X. *Nano Lett.* **2016**, *16* (1), 105−113.

(35) Cheng, G.; Miao, C.; Qin, Q.; Li, J.; Xu, F.; Haftbaradaran, H.; Dickey, E. C.; Gao, H.; Zhu, Y. *Nat. Nanotechnol.* **2015**, *10* (8), 687−691.

(36) Wingert, M. C.; Chen, Z. C. Y.; Dechaumphai, E.; Moon, J.; Kim, J.-H.; Xiang, J.; Chen, R. *Nano Lett.* **2011**, *11* (12), 5507−5513.

(37) Wingert, M. C.; Kwon, S.; Hu, M.; Poulikakos, D.; Xiang, J.; Chen, R. *Nano Lett.* **2015**, *15* (4), 2605−2611.

(38) See Supporting Information for information about nanotube sample types and dimensions, additional TEM images, stress−strain curves, instantaneous and relaxed moduli, creep dependence on initial stress and strain, electron beam exposure, and fracture strength.

(39) Zhu, Y.; Xu, F.; Qin, Q. Q.; Fung, W. Y.; Lu, W. *Nano Lett.* **2009**, *9* (11), 3934−3939.

(40) Wang, Z. L.; Gao, R. P.; Poncharal, P.; de Heer, W. A.; Dai, Z. R.; Pan, Z. W. *Mater. Sci. Eng., C* **2001**, *16* (1−2), 3−10.

(41) Dikin, D. A.; Chen, X.; Ding, W.; Wagner, G.; Ruoff, R. S. *J. Appl. Phys.* **2003**, *93* (1), 226−230.

(42) Polyakov, B.; Antsov, M.; Vlassov, S.; Dorogin, L. M.; Vahtrus, M.; Zabels, R.; Lange, S.; Lõhmus, R. *Beilstein J. Nanotechnol.* **2014**, *5*, 1808−1814.

(43) Freund, L. B.; Suresh, S. *Thin film materials: stress, defect formation, and surface evolution*; 1st ed.; Cambridge University Press: Cambridge, England, 2009; p xviii, 750 pp.

(44) Kizuka, T.; Takatani, Y.; Asaka, K.; Yoshizaki, R. *Phys. Rev. B: Condens. Matter Mater. Phys.* **2005**, *72* (3), 035333.

(45) Hedler, A.; Klaumunzer, S. L.; Wesch, W. *Nat. Mater.* **2004**, *3* (11), 804−809.

(46) Ashtekar, S.; Scott, G.; Lyding, J.; Gruebele, M. *Phys. Rev. Lett.* **2011**, *106* (23), 235501.

(47) EerNisse, E. P. *Appl. Phys. Lett.* **1977**, *30* (6), 290−293.

(48) Doremus, R. H. *J. Appl. Phys.* **2002**, *92* (12), 7619−7629.

(49) Awaji, N.; Ohkubo, S.; Nakanishi, T.; Sugita, Y.; Takasaki, K.; Komiya, S. *Jpn. J. Appl. Phys.* **1996**, *35*, L67.

(50) Watanabe, K.; Kawasaki, T.; Tanaka, H. *Nat. Mater.* **2011**, *10* (7), 512−520.

(51) Novikov, V. N.; Sokolov, A. P. *Nature* **2004**, *431* (7011), 961−963.

(52) Brambilla, L.; Colombo, L.; Rosato, V.; Cleri, F. *Appl. Phys. Lett.* **2000**, *77* (15), 2337−2339.

(53) Shin, J. H.; Atwater, H. A. *Phys. Rev. B: Condens. Matter Mater. Phys.* **1993**, *48* (9), 5964−5972.

(54) Coffa, S.; Priolo, F.; Battaglia, A. *Phys. Rev. Lett.* **1993**, *70* (24), 3756−3759.

(55) Griscom, D. L. *J. Non-Cryst. Solids* **1984**, *68* (2−3), 301−325.

(56) Stallons, J. M.; Iglesia, E. *Chem. Eng. Sci.* **2001**, *56* (14), 4205−4216.

(57) Hemeryck, A.; Richard, N.; Estève, A.; Rouhani, M. D. *J. Non-Cryst. Solids* **2007**, *353* (5−7), 594−598.

(58) Volkert, C. A. *J. Appl. Phys.* **1991**, *70* (7), 3521−3527.

(59) Strauß, F.; Dörrer, L.; Geue, T.; Stahn, J.; Koutsioubas, A.; Mattauch, S.; Schmidt, H. *Phys. Rev. Lett.* **2016**, *116* (2), 025901.

(60) Chen, Y.-C.; Lu, Z.; Nomura, K.-i.; Wang, W.; Kalia, R. K.; Nakano, A.; Vashishta, P. *Phys. Rev. Lett.* **2007**, *99* (15), 155506.

(61) Pradeep, N.; Kim, D.-I.; Grobelny, J.; Hawa, T.; Henz, B.; Zachariah, M. R. *Appl. Phys. Lett.* **2007**, *91* (20), 203114.

(62) Tang, C.; Dávila, L. P. *J. Appl. Phys.* **2015**, *118* (9), 094302.

(63) Egerton, R. F.; Li, P.; Malac, M. *Micron* **2004**, *35* (6), 399−409.

(64) Darwent, B. d. B. *National Bureau of Standards* **1970**, *nsrds-nbs31* (31), 1−62.